



Solid-Phase Upcycling Toward the Production of Ultrahigh-Loading Single-Atom Catalysts

Guanwu Lian¹ | Zefan Du¹ | Yifan Wang¹ | Yelan Xiao² | Mengyao Su³ | Chao Wu⁴ | Yucong Huang¹ | Yuansheng Lin¹ | Jingjing Xiong¹ | Yichen Chen¹ | Shibo Xi⁴ | Wenguang Tu¹ | Zhigang Zou¹ | Zhongxin Chen¹ |

¹School of Science and Engineering, The Chinese University of Hong Kong, Shenzhen, Guangdong, China | ²Shenzhen Key Laboratory of Nano-Biosensing Technology, Marshall Laboratory of Biomedical Engineering, School of Biomedical Engineering, Shenzhen University Medical School, Shenzhen University, Shenzhen, China | ³Department of Applied Physics, Hong Kong Polytechnic University, Hong Kong, China | ⁴Institute of Chemical and Engineering Sciences, Agency for Science, Technology and Research (A*STAR), Jurong Island, Singapore, Singapore

Correspondence: Yelan Xiao (ylxiao@szu.edu.cn) | Zhigang Zou (zouzhigang@cuhk.edu.cn) | Zhongxin Chen (chenzhongxin@cuhk.edu.cn)

Received: 24 February 2025 | Revised: 29 March 2025 | Accepted: 17 April 2025

Funding: This study was supported by University Development Fund Research Start-up Fund from the Chinese University of Hong Kong (Shenzhen), Grant Number: 'UDF01002976'; Shenzhen Science and Technology Program, Grant Number: 'JCYJ20230807114302005', 'JCYJ20240813113559075'; National Natural Science Foundation of China, Grant Number: '22350410375'; Young Scientists Fund of the National Natural Science Foundation of China, Grant Number: '52202306'; Basic and Applied Basic Research Foundation of Guangdong Province, Grant Number: '2024A1515012504'; Shenzhen Key Laboratory of Eco-materials and Renewable Energy, Grant Number: 'ZDSYS20200922160400001'; Guangdong Introducing Innovative and Entrepreneurial Teams, Grant Number: '2019ZT08L101', 'RCTDPT2020-001'; Shenzhen Science and Technology Innovation Program, Grant Number: 'JCYJ20240813142515020'.

Keywords: big-data analysis | dynamic aggregation | single-atom catalysts | solid-phase upcycling | spent catalyst recovery | techno-economic analysis

ABSTRACT

The recovery of valuable transition metals from deactivated catalysts is crucial for alleviating the challenges of resource scarcity and environmental pollution. Guided by AI-powered big data analysis, we identified an important research gap in the sustainable recovery of early transition metals and proposed a solid-phase upcycling strategy to transform waste catalysts into highly valuable single-atom catalysts (SACs). This involves a heat-induced redispersion of metal aggregates into single atoms on the polycrystalline carbon nitride (PCN) support, producing highly active M_1 -PCN SACs up to 20 wt% (M = Cu, Fe, Co, and Ni). Subsequent technoeconomic analysis confirms a two-thirds reduction in production cost and greenhouse gas emissions compared to conventional hydrometallurgical and pyrometallurgical processes, thus paving a new path in the development of sustainable technologies for metal recovery.

1 | Introduction

The recovery of metals from various sources, particularly spent catalysts and electronic waste, has gained significant attention in recent years due to the growing demand for transition metals and the environmental concerns associated with mining and waste disposal [1–3]. For instance, the world would mine 8700 million

tons of Cu from 2020 to 2100, far more than the reserve of 2000 million tons [4].

Pyrometallurgical and hydrometallurgical processes are two cornerstones in traditional metal recovery. The former involves direct high-temperature smelting to reduce transition metals to achieve $\sim 100\%$ metal recovery, while the latter also affords high

Guanwu Lian, Zefan Du, and Yifan Wang contributed equally to this work.

This is an open access article under the terms of the Creative Commons Attribution License, which permits use, distribution and reproduction in any medium, provided the original work is properly cited.

© 2025 The Author(s). Aggregate published by SCUT, AIEI and John Wiley & Sons Australia, Ltd.

yields by incorporating lengthy acid/base-leaching processes [5–7]. These affordable yet unsustainable approaches necessitate the exploration of advanced, green recycling methods such as electrochemical [8–11], photochemical [12–15], and other more sustainable alternatives with specifically designed materials [14, 16, 17]. For instance, Bian et al. reported a photocatalytic process to retrieve seven precious metals from waste [15]. Ding et al. also identified an advanced oxidation process using peroxydisulfate to recover palladium and gold [18]. Moreover, to extend the recycling chain and increase the recycling revenue, some methods were developed to upcycle materials from waste to value-added products by regulating chemical structures and endowing properties for catalytic, optical, and other applications [19–21].

Among these approaches, solid-phase recovery is promising for extracting valuable metals from spent catalysts by selectively binding and concentrating metals with solid materials, which offers advantages in reduced chemical consumption and potential for integration into existing industrial processes [22–24]. Unfortunately, critical challenges remain in the complexity of spent catalyst matrices and the economic viability [24]. The solid-phase upcycling of spent catalysts into advanced catalysts, such as single-atom catalysts (SACs) with maximum atom utilization efficiency, would demonstrate high practical feasibility [25, 26].

Herein, we proposed a solid-phase upcycling strategy based on artificial intelligence (AI)-powered big data analysis of existing metal recovery methods. Waste nanoparticle catalysts were transformed into ultrahigh-loading SACs by solid-phase redispersion of metal atoms on polymeric carbon nitride (PCN) via ball milling and subsequent heat-induced redispersion. The economic feasibility was verified by a preliminary techno-economic analysis (TEA) in CatCost (from the US Department of Energy, DOE) [27, 28]. The upcycled Cu SACs exhibited excellent catalytic performance toward the C—N coupling reaction with an isolated yield of 71%, thus opening up a new path in the development of sustainable technologies for metal recovery.

2 | Results and Discussion

2.1 | Big Data Analysis of the Literature

We employed an AI-powered rule-based approach [29–31] (details in Supporting Information) to analyze the existing metal recovery methods. A database of literature containing 201,371 papers from different esteemed publishers, including ACS, RSC, Wiley, and Nature, was obtained. Using keywords (such as pyrometallurgical and hydrometallurgical), 5732 papers on the topic of catalyst recovery were identified and further narrowed down into three categories (pyrometallurgy, hydrometallurgy, and others) in Figure 1. Our analysis indicates that hydrometallurgy is the most prominent method for spent catalysts, accounting for 76.0% of the analyzed pathways, while pyrometallurgy represents a smaller portion at 7.5% in Figure 1B. A statistical analysis of the pH levels in hydrometallurgy is presented, suggesting the dominance of the acid-leaching processes (70.0%) against alkaline (16.0%) and neutral (8.0%) treatments in Figure 1C. This agrees well with the systematic review by Gao et al., where strongly oxidizing acids such as nitric acid and hot concentrated sulfuric acid are commonly employed to extract noble metals in the spent catalysts [3]. Innovative pyrometallurgical approaches such as flash Joule heating and microwave smelting with reduced energy consumption have also gained increasing attention [3, 5]. The number of papers related to the top 10 metal elements involved in metal recovery is shown in Figure 1D. The data reveals that early transition metals such as copper (13.5%), nickel (10.2%), cobalt (20.2%), and iron (15.1%) are the most frequently studied elements, while the precious metals (platinum, palladium, gold, silver, and ruthenium) are also the focus of recovery given their economic value and environmental significance. This highlights the importance of a universal recycling approach for early transition metals with minimum waste generation and affordable cost. Our AI big-data analysis offers a comprehensive understanding of the existing metal recovery strategies, guiding us toward developing a solid-phase upcycling method for early transition metals (Fe, Co, Ni, Cu), accounting for nearly 60% of the reported literature.

2.2 | Solid-Phase Upcycling Toward the Production of SACs

The solid-phase recovery process of the spent catalyst is shown in Figure 2A. The spent catalyst from the C—N coupling and nitrate reduction reactions (details in Supporting Information) or a simulated sample of CuO was first physically mixed with a nitrogen-rich support (PCN) via ball milling for homogeneous mixing, followed by heat-induced redispersion to transform copper oxides into the desired Cu₁-PCN catalyst with a maximum loading of up to 20 wt%. Such transformation is analogous to the conventional synthesis of SACs on the PCN supports and can be visualized by an obvious color change from grey to brown (or light brown), depending on the metal loading [32, 33]. A major benefit of our method lies in the reduced thermal treatment steps to synthesize ultrahigh-loading SACs compared to conventional methods.

The successful upcycling of spent catalysts into Cu₁-PCN SACs was evidenced by X-ray diffraction (XRD) patterns. As shown in Figure 2B, the initial ball milling is a physical mixing process and does not involve mechanochemical reactions between copper oxides and PCN. The characteristic peaks of CuO at 32.5°, 35.5°, 38.7°, and 48.8° disappear after heat treatment with PCN at 550°C, leaving a broad peak at 27.6° corresponding to the (002) plane of PCN in the Cu₁-PCN samples. The absence of the nanoparticle peak implies the uniform dispersion of Cu atoms across the PCN matrix regardless of metal loading [32, 33]. The actual Cu loading of various samples from 7 to 20 wt% was determined by inductively coupled plasma optical emission spectrometry (ICP-OES) in Table S1. Ex situ XRD experiments coupled with stepwise heating in thermogravimetric analysis (TGA) were further performed to investigate the metal recovery mechanism, showcasing a dynamic reduction and redispersion process of copper oxides from 250°C to 550°C in Figure 2C. The metal reduction occurs at 350°C and above, leading to the appearance of a characteristic peak of Cu₂O at 36.3°. Further reduction at 450°C results in the formation of metallic species (Cu nanoparticles), as indicated by the tiny peak at ~43.3°. These XRD signals related to copper oxides and metallic species completely vanish after treatment at 550°C, leaving only one peak related to the PCN support due to heat-induced redispersion into atomically dispersed species. This is probably attributed to the higher thermodynamic stability of

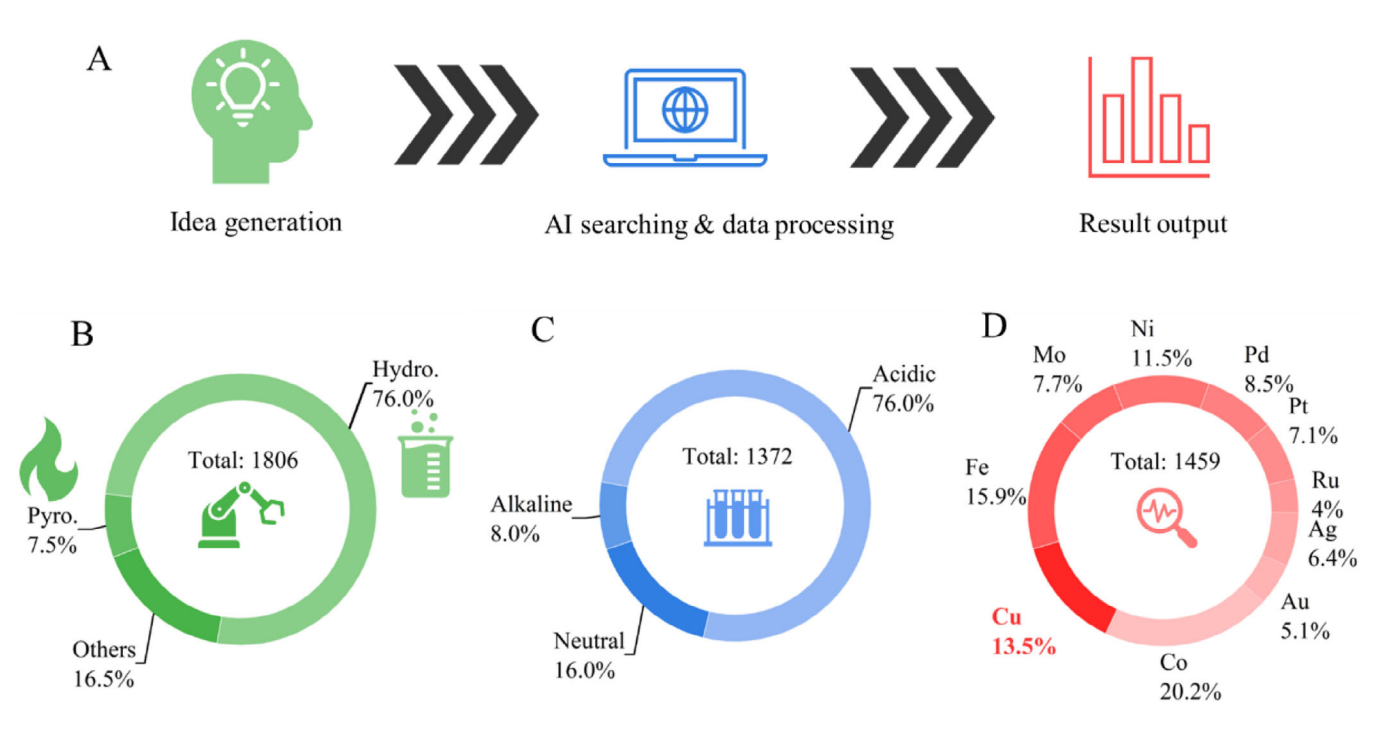


FIGURE 1 | Big-data analysis of the recycling pathways for the spent catalysts. (A) The AI-assisted literature analysis process. (B) Analysis of three major recycling pathways in the database. (C) The statistics analysis of pH in hydrometallurgy recycling. (D) The number of papers related to the top 10 metal elements in metal recovery. Pyro: pyrometallurgy, Hydro: hydrometallurgy.

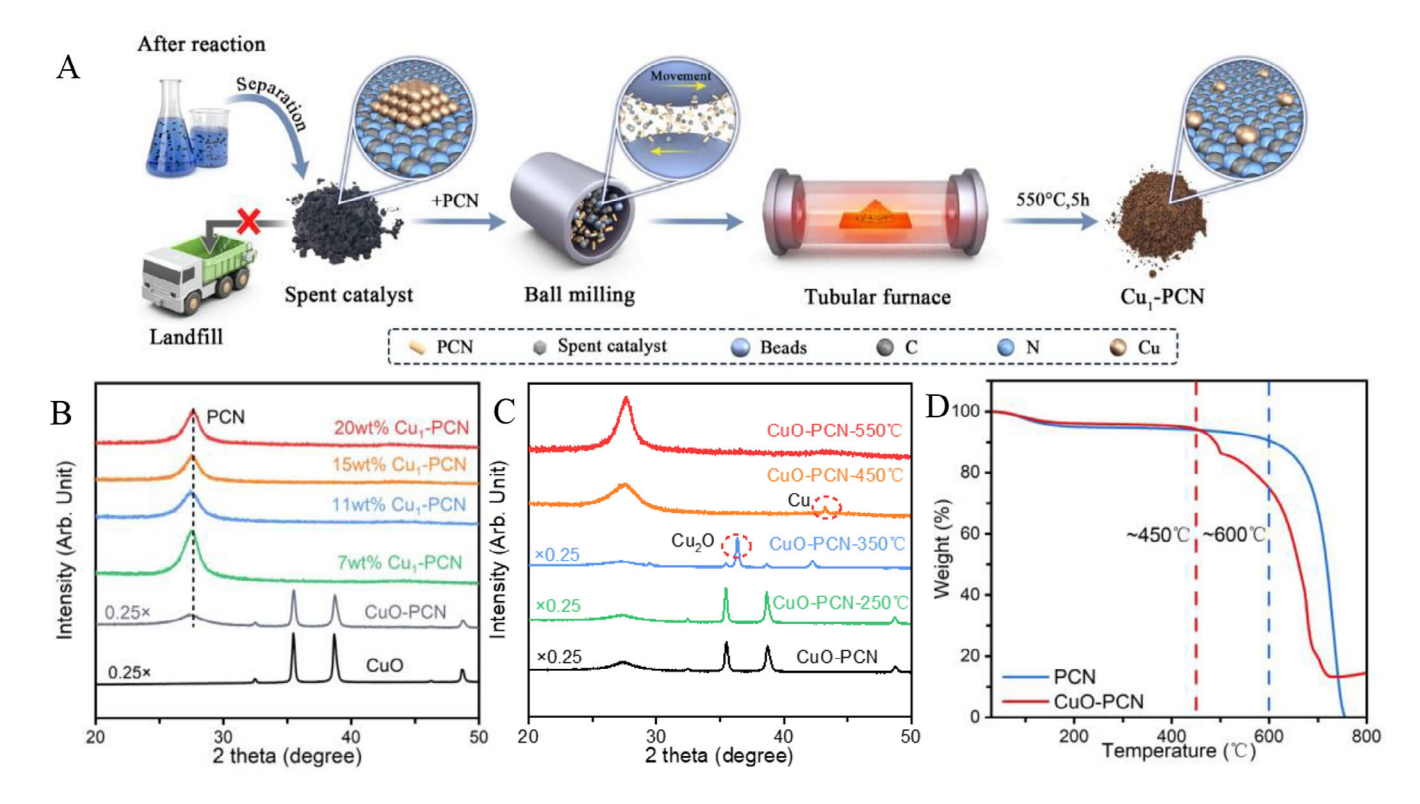


FIGURE 2 Solid-phase upcycling into Cu_1 -PCN catalyst. (A) Schematic showing of the solid-phase upcycling process. (B) XRD patterns of the precursor (CuO) and as-synthesized Cu_1 -PCN catalysts with various loadings. (C) Ex-situ XRD measurements of the solid-phase upcycling process using the CuO and PCN mixture at various temperatures. (D) TGA curves of CuO-PCN and PCN. CuO was chosen as a simulated sample. Data from the spent catalysts after the C—N coupling and nitrate reduction reactions can be found in the Figure 4 and Supporting Information.

on Wiley Online Library for rules of use; OA articles are governed by the applicable Creative Commons License

26924560, 2025, 8, Downloaded from

nelibrary.wiley.com/doi/10.1002/ag12.70052 by HONG KONG POLYTECHNIC UNIVERSITY HU NG HOM, Wiley Online Library on [06/11/2025]. See the Term

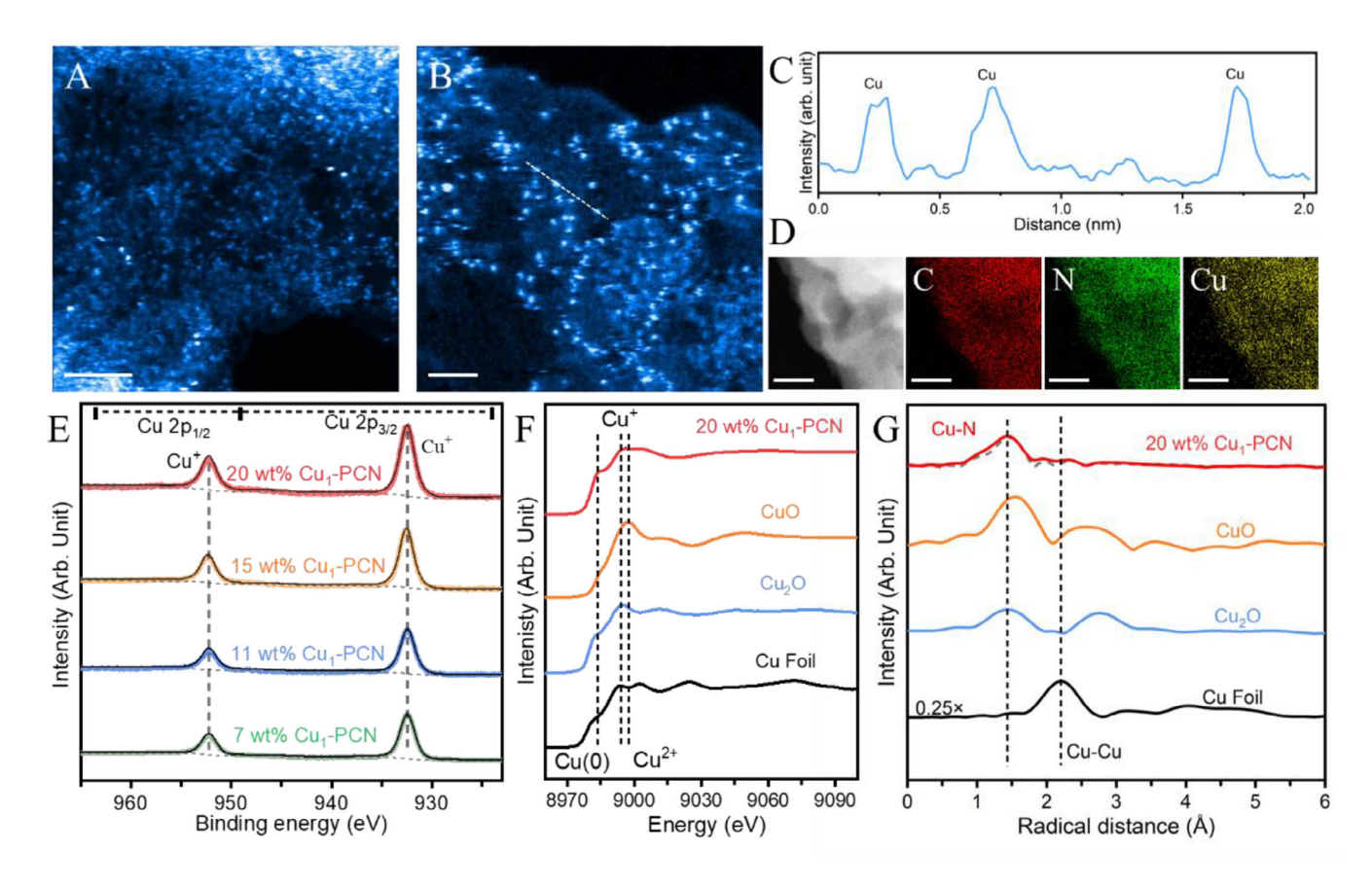


FIGURE 3 Characterization of the Cu_1 -PCN catalyst. (A–C) Atomic resolution HAADF-STEM images of the 20wt% Cu_1 -PCN and the corresponding line profile. (D) High-resolution TEM image and EDS mapping of Cu, C, and C0 for the 20wt% Cu_1 -PCN. (E) XPS of the Cu_1 -PCN catalysts with various loadings. (F) Cu C0 for Cu1 for Cu2 for Cu3 for Cu3 for Cu4 for Cu5 for Cu6 for Cu7 for Cu8 for Cu9 for Cu9

single atoms against nanoparticles on the PCN support, where similar observations have been found on N-rich supports and reducible metal oxides (CeO_2 , TiO_2 , etc.) [34]. Likewise, TGA results confirm that the weight loss begins at around 450°C for the physical mixture of CuO and PCN, while pure PCN is thermally stable in argon until 600°C in Figure 2D. This suggests a stepwise redispersion process involving cupric oxide (Cu_2O) and metallic species for producing Cu_1 -PCN.

The atomic dispersion and morphology of Cu₁-PCN SACs were characterized by scanning transmission electron microscopy in the high-angle annular dark-field mode (HAADF-STEM) in Figures 3A,B, and S1. The isolated Cu atoms in Cu₁-PCN appear as bright spots in the matrix. No particle aggregation was observed in HAADF-STEM even at an ultrahigh metal loading of 20 wt%, which agrees well with the absence of Cu particle peak in XRD patterns. The corresponding intensity line profile along the white line in Figure 3C confirms these are Cu single atoms rather than dimers or trimers. The oxidation state of Cu single atoms is then verified by electron energy loss spectroscopy (EELS) in Figure S2A. Relative to Cu²⁺ at 932 eV and Cu⁺ at 935 eV, our 20 wt% Cu₁-PCN shows a partially oxidized state ($Cu^{\sigma+}$) and is distinguished from metallic Cu (from Cu grid) in the Cu L_3 edge [35]. Energydispersive X-ray spectroscopy (EDS) analysis in Figures 3D and S2 illustrates the uniform dispersion of Cu species across the sample.

Further confirmation of the oxidation state and coordination environment of Cu species was conducted by X-ray photoelectron spectroscopy (XPS) and X-ray absorption spectroscopy (XAS) [33]. Regardless of metal loading, all four samples of Cu₁-PCN exhibit only a partially oxidized state (Cu $^{\sigma+}$, $\sigma = 0 \sim 1$) with the spinorbit doublets of Cu 2p_{3/2} and 2p_{1/2} at 932.7 and 952.5 eV in the XPS spectra in Figure 3E [36]. Similarly, the K-edge X-ray absorption near-edge structure (XANES) spectra in Figure 3F also reveal a partial oxidation state of Cu in the 20 wt% Cu₁-PCN that is distinct from referencing samples of CuO, Cu₂O, and Cu foil [37]. No Cu-Cu metallic peak could be found in the Fourier-transformed extended X-ray absorption fine structure (FT-EXAFS). A prominent peak at ~1.5 Å from the scattering of the first coordination shell (Cu-N) is visualized for all the Cu₁-PCN samples in Figure 3G and Table S2, in contrast to the chloride (~1.9 Å), oxides (significant scattering of the second coordination shell at $\sim 2.8 \,\text{Å}$), and metallic species ($\sim 2.2 \,\text{Å}$) [32]. The fitted curve (dotted) confirms a Cu-N coordination number of ~ 2.0 that agrees with previous reports. The wavelength transform (WT)-EXAFS in Figure S3 also displays the most intensive peak at ~1.5 Å of Cu-N. The influence of particle size on the efficiency of solid-phase recovery was evaluated by a systematic experiment in Figure S4, where the primary function of ball milling is to ensure the homogeneous mixing of the samples. Combined with STEM, XPS, and XRD data, we conclude the successful upcycling into the Cu₁-PCN SACs.

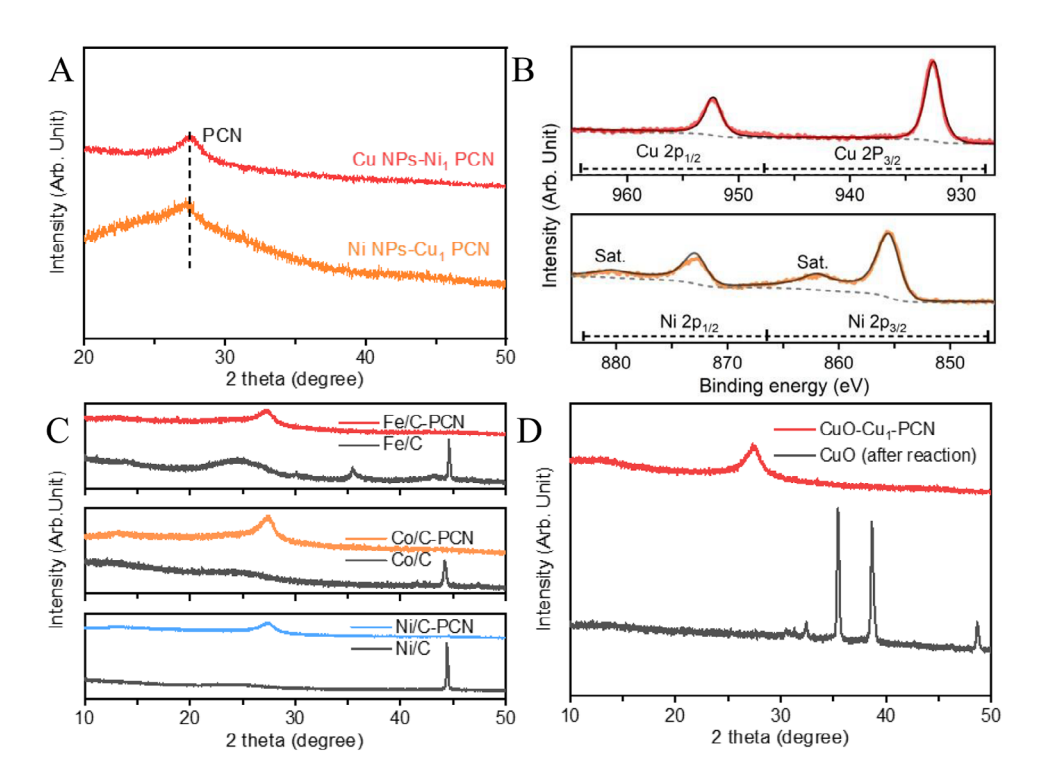


FIGURE 4 The universal applicability of solid-phase upcycling. (A) XRD patterns and (B) XPS spectra of the bimetallic samples. (C) Applicability toward the upcycling of iron, cobalt, and nickel catalysts. (D) XRD patterns of the recovered CuO catalyst after the C—N coupling reaction.

2.3 | Material Scope and Techno-Economic Analysis

Extensions to other raw materials, such as nano Cu powder, Cu₂O, Cu clusters, and commercial Cu/C catalysts, were also examined. The XRD and Cu FT-EXAFS spectra in Figure S5 shows similar results to the one using CuO as the raw material, indicating our upcycling method can be extended to a broad scope of Cu substrates. Bimetallic SACs of Cu and Ni could be synthesized using Cu nanoparticles (or Ni nanoparticles) and Ni-PCN (or Cu-PCN) in good yield. Both bimetallic samples only show a characteristic peak related to PCN in the XRD patterns without particle aggregation in Figure 4A [33]. The corresponding XPS spectra reveal partially oxidized Cu⁺ and Ni^{σ +} ($\sigma = 1 \sim$ 2) species in the bimetallic samples, while their coexistence is confirmed by the uniform dispersion on PCN in the EDS mapping in Figures 4B and S6. Furthermore, we have also examined the applicability toward other early transition metals (Fe, Co, and Ni). The disappearance of prominent peaks related to Fe, Co, and Ni particles in the XRD patterns in Figure 4C suggests successful redispersion into the corresponding M_1 -PCN (M = Fe, Co, and Ni). Finally, the actual spent catalysts (predominantly constituted of CuO) after the carbon-nitrogen (C-N) coupling and electrochemical nitrate reduction (NO3RR) reactions could be effectively recovered by our solid-phase recovery. The XRD and XPS results in Figures 4D and S7 are analogous to the ones using CuO as the simulated sample in Figures 2 and 3.

To assess the economic feasibility of our solid-phase upcycling, we have calculated the production cost and greenhouse gas emission (GHG) compared with the traditional pyrometallurgical and hydrometallurgical processes from the published data in battery recycling [38, 39]. As shown in the detailed synthetic steps of each

method in Figure 5, our strategy is advantageous in reducing the number of steps in metal recycling and enabling the production of value-added products such as SACs. Other benefits include lower environmental impact with less chemical waste generation, reduced energy consumption compared to pyrometallurgy due to operation at lower temperatures, and a broad scope of raw materials for recovery [1, 3].

Since the production cost is one of the most important considerations of practical metal recovery, we employ a simplified step method (CatCost version 1.1.0) from the US Department of Energy (DOE) to evaluate the production cost of 20 wt% Cu₁-PCN from the spent catalysts via hydrometallurgy, pyrometallurgy, and solid-phase upcycling [27, 28]. As shown in Table 1, our strategy shows the best cost-effectiveness for industrial-scale production. The production cost of 20 wt% Cu₁-PCN is estimated to be \$34.40 per kilogram, which is much lower than that of commercial supported catalysts at a similar metal loading (such as \$47.02 per kilogram for 21 wt% Ni/Al₂O₃) [28]. Despite similar raw material costs (~\$8 kg⁻¹), the processing cost of our method is only about one-third of the corresponding values in hydrometallurgy and pyrometallurgy (14.40 vs. 43.20 and \$41.90 per kilogram), highlighting the need to minimize synthetic steps. This agrees well with the published data on 20.8 wt% Ni₁/PCN, whose process cost (\$30.18/kg) is double that of the material cost, which adds more complexity and uncertainty to scale up [33]. A comparative analysis of commercially available Cu-based catalysts was conducted to evaluate the economic viability of our synthetic approach, as shown in Tables S3 and S4. Specifically, the widely used 10 wt% Cu/C catalyst (purchased from Fuel Cell Store and MTI Cooperation) exhibits a market price exceeding \$195 per gram, as documented in current industrial procurement records. This cost differential underscores the economic feasibility of our

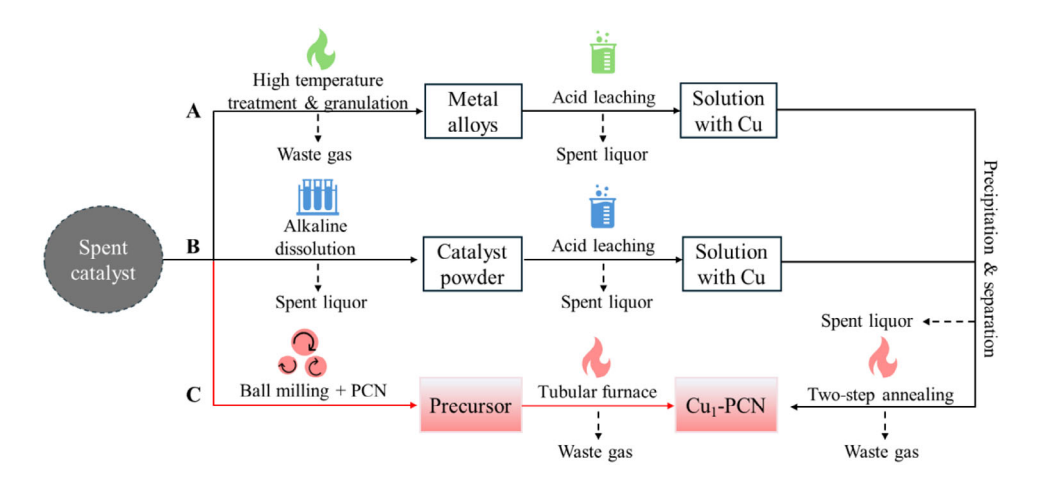


FIGURE 5 The production flow of Cu₁-PCN in various pathways. (A) Pyrometallurgy, (B) hydrometallurgy, and (C) solid-phase upcycling. Our solid-phase approach prevents corrosive solvents and minimizes the heating steps.

TABLE 1 Cost evaluation and GHG emission of the upcycled 20wt% Cu₁-PCN.

Method Cost (\$/kg)	Pyrometallurgy	Hydrometallurgy	Solid-phase upcycling
Processing Steps	43.20	41.90	14.40
Overheads			
1. General and administrative	4.32	4.19	1.44
2. Sales, admin., research, distribution	4.75	4.61	1.59
3. Selling margin	31.90	30.90	10.65
Step method total	84.10	81.6	28.10
Raw materials	8.82	8.47	7.90
Spent catalyst value (SCV)	1.67	1.67	1.67
Net catalyst cost	88.70	90.90	34.40
GHG emission (kg/kg catalyst)	53.00	51.40	17.70

approach, positioning it as a competitive alternative for practical applications.

Meanwhile, the GHG emissions were also estimated according to the DOE document (Everbatt2020) [40]. The GHG emission of solid-phase upcycling is roughly one-third of that in the other two methods (17.70 vs. 53.00 and 51.40 kg GHG per kg catalyst) owing to lower operation temperature and reduced synthetic steps. This value is slightly lower than the GHG emission of traditional manufacturing of 10 wt% Cu/C catalysts at high temperatures (~22.5 kg GHG per kg catalyst). In this regard, our solid-phase upcycling production of ultrahigh-loading SACs is highly promising in view of the production cost and GHG emissions.

2.4 | Catalytic Performance of the Cu₁-PCNs

We selected the carbon–nitrogen coupling reaction between 4-bromoacetophenone and imidazole as a model reaction to evaluate the catalytic performance of Cu₁-PCN SACs. According to our previous works, such a reaction is known to be sensitive to the coordination environment of individual Cu sites through

a cooperative bridge-coupling pathway with dynamic Cu—Cu bonding [32, 41]. Given our prime focus on metal recovery, the structure–property relationship on the SAC-mediated C—N coupling is not detailed here.

As shown in Figure 6 and Table S5, the isolated yield of the C-N coupling reaction increases with higher Cu loadings, giving the highest yield of 71% when 20 wt% Cu₁-PCN was used. This is in accordance with the dinuclear pathway, where a shorter inter-metal distance in ultrahigh-loading SACs promotes the cross-coupling reactions [32, 41]. Particle aggregation occurs at higher Cu loadings (>27 wt%), leading to a decline in catalytic performance due to a lower metal utilization efficiency of nanoparticles than SACs in Figure S8. In contrast, the pure PCN sample shows no activity to the C-N coupling due to the lack of catalytically active metal sites. Control samples of 10 wt% Cu/C, CuBr, and CuO exhibit relatively low activity and leaching resistance compared to Cu₁-PCNs. The structure of the product is further confirmed by nuclear magnetic resonance spectroscopy (NMR) in Figure S9. We have also verified the catalytic performance of monometallic Ni₁-PCN and bimetallic Cu₁Ni₁-PCN toward the C-N coupling. As shown in Figure S10, 6 wt% Ni₁-PCN and Cu₁Ni₁-PCN (9 wt% Cu + 6 wt% Ni) exhibited

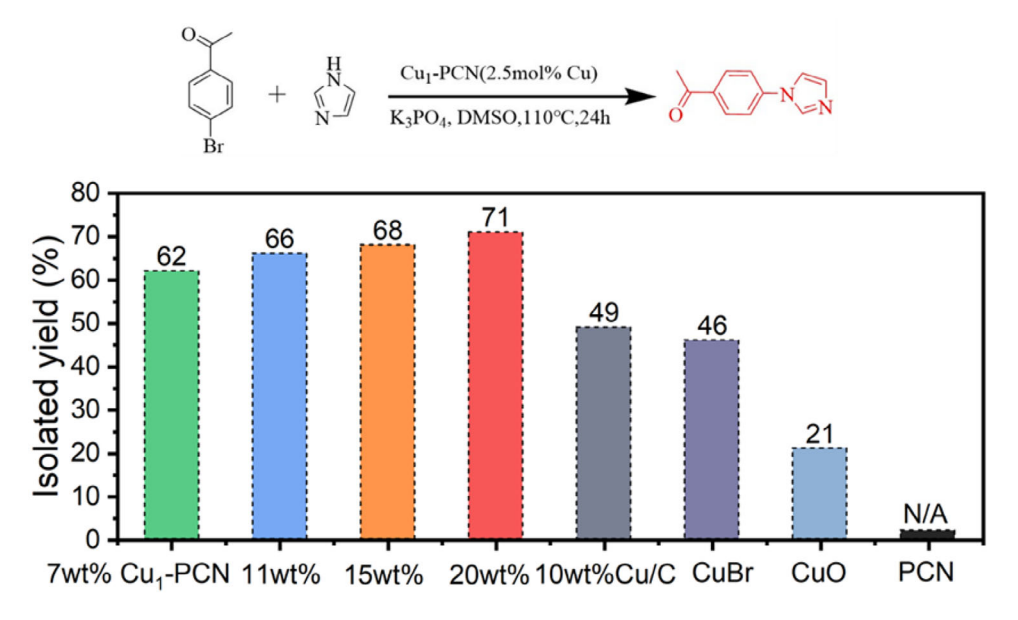


FIGURE 6 | Catalytic performance of Cu_1 -PCN in the C-N coupling reaction. Catalyst screening for the C-N coupling reaction using 4-bromoacetophenone and imidazole as reactants. The reaction equation is also provided.

isolated yields of 31% and 58%, which are inferior to 7 wt% Cu_1 -PCN (62%) per metal loading. A plausible explanation is that the Cu—Cu pair has better catalytic activity than the Ni—Ni pair toward the C—N coupling. The introduction of secondary metal in the bimetallic systems leads to the formation of heteronuclear Cu—Ni pairs and reduces the density of more reactive Cu—Cu pairs, leading to a reduced performance in the Cu_1Ni_1 -PCN samples.

The catalyst stability was evaluated by five successive runs in Figure S11, where slightly lower yields could be observed in the fourth and fifth runs due to catalyst loss during catalyst separation steps. The structure of the spent Cu₁-PCN was further examined by XRD in Figure S12, where good crystallinity of PCN can be retained without obvious aggregation of Cu in the spent catalyst. In contrast, the metal leaching in high-loading samples (from nanoparticles) will reduce the cycling stability in the long term. The spent catalyst could be regenerated via a similar approach. It should be pointed out that our solid-phase recovery involves a heat-induced re-dispersion (atomization) process of the metal aggregates. This is precisely the reverse process of heat-induced aggregation in catalyst degradation, thus closing the loop in the whole life cycle of metal catalysts. The metal loading and coordination environment of the regenerated SACs can also be finely tuned by the usage and type of PCN supports, which facilitates the customized design of novel SACs for cross-coupling reactions through favorable metal-support interaction.

3 | Conclusion

In conclusion, we have developed a solid-phase upcycling strategy for the cost-effective transformation of the spent nanocatalysts into ultrahigh-loading SACs. This involves ball milling and subsequent atomization at high temperatures to redisperse the metal aggregates into single atoms on the polycrystalline carbon nitride support. Based on big-data analysis and TEA, our strategy

is superior to conventional pyrometallurgy and hydrometallurgy approaches in terms of much lower production cost and GHG emission (\$33.40 and 17.7 kg GHG per kg catalyst) owing to a reduced number in synthetic steps. The as-obtained Cu SACs are highly catalytically active toward the C—N coupling with an isolated yield of 71%, thus offering a promising low-cost pathway for recycling metal catalysts in the future.

4 | Experimental Methods

4.1 | Synthesis of PCN

A certain amount of dicyandiamide was loaded into a crucible and heated to 550°C for 4 h in a muffle furnace at a heating rate of 2.3°C min⁻¹ in ambient. After cooling to room temperature, the obtained solid was further calcined in static air at 500°C for 3 h at 5°C min⁻¹ to prepare the exfoliated PCN.

4.2 | Solid-Phase Upcycling Into the Cu₁-PCN SAC

Commercial CuO was used as the simulated sample for concept demonstration. For the typical synthesis of 20 wt% $\rm Cu_1$ -PCN upcycling from CuO, 0.22 g of CuO was mixed with 1 g of exfoliated PCN by ball milling for 2 h at 400 rpm. The obtained mixture was calcined under 100 sccm Ar in a tubular furnace at 550°C for 5 h at 2.3°C min⁻¹. Brownish $\rm Cu_1$ -PCN powder was obtained after cooling down and washing with ethanol and water. The applicability of solid-phase upcycling toward actual samples was also examined. The spent catalysts from the C—N coupling and nitrate reduction reactions can be upcycled into $\rm Cu_1$ -PCN in a similar protocol.

4.3 | The C-N Coupling Using Cu₁-PCN

0.20 mmol of 4-bromoacetophenone, 0.24 mmol of imidazole, 0.40 mmol of K_3PO_4 , and 2.5 mol% Cu_1 -PCN (regarding the metal)

were added into a pre-dried reaction tube containing 1 mL of anhydrous dimethyl sulfoxide (DMSO) and sealed with a Teflon-lined screw cap in the glove box. Then, the reaction tube was removed from the glove box and heated in an oil bath at 110°C for 24 h. After cooling down to room temperature, the solid content was removed by filtration. The liquid residue was extracted by ethyl acetate and water three times and concentrated by rotary evaporation. The pure product was obtained by silica gel column chromatography from concentrated residue and verified by ¹H NMR.

4.4 | Material Characterization

The following equipment was used: XPS (Thermo Scientific Nexsa), XRD (Rigaku Smartlab with a PhotonMax high-flux 9 kW rotating anode X-ray source), ICP-OES (Agilent 720ES), TEM (JEOL JEM-F200), TGA (Netzsch TG 209 F3), NMR (Bruker Advanced 500 MHz), STEM (JEOL ARM200F equipped with ASCOR probe corrector at 80 kV), EELS (200 kV by a Gatan Quantum ER system with an exposure time of 40 s), and EDS (200 kV by an Oxford Aztec EDS system). XAS data was collected at Singapore Synchrotron Light Sources (SSLS) [42]. Data analysis and simulation were conducted on the Demeter software package (Version 0.9.23) [43].

Author Contributions

G.L. conceived the research, synthesized the materials, conducted the techno-economic analysis, and wrote the draft under the supervision of Z.C.; Z.D., G.L., and Y.X. conducted catalytic experiments; Big-data analysis was performed by Y.W. under the supervision of W.T. and Z.Z.; XAS measurements and data processing were conducted by C.W. and S.X.; STEM characterization and data analysis were conducted by M.S.; Y.H., Y.L., J.X., and Y.C. assisted with materials characterization and data analysis. All authors discussed and commented on the manuscript.

Acknowledgments

Z. C. acknowledges the University Development Fund, Research Start-up Fund (UDF01002976) from the Chinese University of Hong Kong (Shenzhen), the National Natural Science Foundation of China (22350410375), the Shenzhen Science and Technology Program (JCYJ20230807114302005 and JCYJ20240813113559075), the Guangdong Basic and Applied Basic Research Foundation (2024A1515012504). We appreciate the Young Scientists Fund of the National Natural Science Foundation of China (52202306), Guangdong Introducing Innovative and Entrepreneurial Teams (2019ZT08L101 and RCTDPT2020-001), and the Shenzhen Key Laboratory of Eco-materials and Renewable Energy (ZDSYS20200922160400001) and Shenzhen Science and Technology Program (JCYJ20240813142515020).

Conflicts of Interest

The authors declare no conflicts of interest.

Data Availability Statement

All data are available from the authors upon reasonable request.

References

1. A. Zupanc, J. Install, M. Jereb, and T. Repo, "Sustainable and Selective Modern Methods of Noble Metal Recycling," *Angewandte Chemie*

International Edition 62 (2023): e202214453, https://doi.org/10.1002/anie. 202214453

- 2. Y. Chen, Q. Qiao, J. Cao, H. Li, and Z. Bian, "Precious Metal Recovery," *Joule* 5 (2021): 3097–3115, https://doi.org/10.1016/j.joule.2021.11.
- 3. Y. Wei, W. Zhang, and J. Gao, "Trash or Treasure? Sustainable Noble Metal Recovery," *Green Chemistry* 26 (2024): 5684–5707, https://doi.org/10.1039/d3gc04950g.
- 4. D. A. Singer, "Long-Term Copper Production to 2100," *Mathematical Geosciences* 56 (2023): 711–722, https://doi.org/10.1007/s11004-023-10111-8.
- 5. W. Chen, J. Chen, K. V. Bets, et al., "Battery Metal Recycling by Flash Joule Heating," *Science Advances* 9 (2023): eadh5131, https://doi.org/10.1126/sciadv.adh5131.
- 6. M. K. Jha, J.-C. Lee, M.-S. Kim, J. Jeong, B.-S. Kim, and V. Kumar, "Hydrometallurgical Recovery/Recycling of Platinum by the Leaching of Spent Catalysts: A Review," *Hydrometallurgy* 133 (2013): 23–32, https://doi.org/10.1016/j.hydromet.2012.11.012.
- 7. G. Liang and Z. Qu, "Insight Into Pyrometallurgical Recovery of Platinum Group Metals From Spent Industrial Catalyst: Co-Disposal of Industrial Wastes," *ACS ES&T Engineering* 3 (2023): 1532–1546, https://doi.org/10.1021/acsestengg.3c00129.
- 8. A. V. Oladeji, J. M. Courtney, M. Fernandez-Villamarin, and N. V. Rees, "Electrochemical Metal Recycling: Recovery of Palladium From Solution and In Situ Fabrication of Palladium-Carbon Catalysts via Impact Electrochemistry," *Journal of the American Chemical Society* 144 (2022): 18562–18574, https://doi.org/10.1021/jacs.2c08239.
- 9. S. Cotty, J. Jeon, J. Elbert, V. S. Jeyaraj, A. V. Mironenko, and X. Su, "Electrochemical Recycling of Homogeneous Catalysts," *Science Advances* 8 (2022): eade3094, https://doi.org/10.1126/sciadv.ade3094.
- 10. S. R. Cotty, N. Kim, and X. Su, "Electrochemically Mediated Recovery and Purification of Gold for Sustainable Mining and Electronic Waste Recycling," *ACS Sustainable Chemistry & Engineering* 11 (2023): 3975–3986, https://doi.org/10.1021/acssuschemeng.3c00227.
- 11. Y. Su, A. Berbille, X.-F. Li, et al., "Reduction of Precious Metal Ions in Aqueous Solutions by Contact-Electro-Catalysis," *Nature Communications* 15 (2024): 4196, https://doi.org/10.1038/s41467-024-48407-w.
- 12. J. Cao, Y. Chen, H. Shang, et al., "Aqueous Photocatalytic Recycling of Gold and Palladium From Waste Electronics and Catalysts," *ACS ES&T Engineering* 2 (2022): 1445–1453, https://doi.org/10.1021/acsestengg.1c00505
- 13. Y. Chen, S. Guan, H. Ge, et al., "Photocatalytic Dissolution of Precious Metals by TiO(2) Through Photogenerated Free Radicals," *Angewandte Chemie International Edition* 61 (2022): e202213640, https://doi.org/10.1002/anie.202213640.
- 14. H. Yang, J. Xu, H. Cao, J. Wu, and D. Zhao, "Recovery of Homogeneous Photocatalysts by Covalent Organic Framework Membranes," *Nature Communications* 14 (2023): 2726, https://doi.org/10.1038/s41467-023-38424-6.
- 15. Y. Chen, M. Xu, J. Wen, et al., "Selective Recovery of Precious Metals Through Photocatalysis," *Nature Sustainability* 4 (2021): 618–626, https://doi.org/10.1038/s41893-021-00697-4.
- 16. Y. Hong, D. Thirion, S. Subramanian, et al., "Precious Metal Recovery From Electronic Waste by a Porous Porphyrin Polymer," *Proceedings of the National Academy of Sciences of the United States of America* 117 (2020): 16174–16180, https://doi.org/10.1073/pnas.2000606117.
- 17. A. Zadehnazari, F. Auras, A. A. Altaf, et al., "Recycling E-Waste Into Gold-Loaded Covalent Organic Framework Catalysts for Terminal Alkyne Carboxylation," *Nature Communications* 15 (2024): 10846, https://doi.org/10.1038/s41467-024-55156-3.
- 18. A. Ding, M. Li, C. Liu, et al., "Recovering Palladium and Gold by Peroxydisulfate-Based Advanced Oxidation Process," *Science Advances* 10 (2024): eadm9311, https://doi.org/10.1126/sciadv.adm9311.

- 19. D. Xia, C. Lee, N. M. Charpentier, Y. Deng, Q. Yan, and J.-C. P. Gabriel, "Drivers and Pathways for the Recovery of Critical Metals From Waste-Printed Circuit Boards," *Advanced Science* 11 (2024): e2309635, https://doi.org/10.1002/advs.202309635.
- 20. S. S. Shin, Y. Jung, S. Jeon, et al., "Efficient Recovery and Recycling/Upcycling of Precious Metals Using Hydrazide-Functionalized Star-Shaped Polymers," *Nature Communications* 15 (2024): 3889, https://doi.org/10.1038/s41467-024-48090-x.
- 21. J. Wang, K. Jia, J. Ma, et al., "Sustainable Upcycling of Spent LiCoO $_2$ to an Ultra-Stable Battery Cathode at High Voltage," *Nature Sustainability* 6 (2023): 797–805, https://doi.org/10.1038/s41893-023-01094-9.
- 22. J. J. Roy, S. Rarotra, V. Krikstolaityte, et al., "Green Recycling Methods to Treat Lithium-Ion Batteries E-Waste: A Circular Approach to Sustainability," *Advanced Materials* 34 (2022): e2103346, https://doi.org/10.1002/adma.202103346.
- 23. J. Shi, S.-Q. Peng, B. Kuang, et al., "Porous Polypyrrolidines for Highly Efficient Recovery of Precious Metals Through Reductive Adsorption Mechanism," *Advanced Materials* 36 (2024): e2405731, https://doi.org/10.1002/adma.202405731.
- 24. C. Stinn and A. Allanore, "Selective Sulfidation of Metal Compounds," *Nature* 602 (2022): 78–83, https://doi.org/10.1038/s41586-021-04321-5.
- 25. X. Liang, N. Fu, S. Yao, Z. Li, and Y. Li, "The Progress and Outlook of Metal Single-Atom-Site Catalysis," *Journal of the American Chemical Society* 144 (2022): 18155–18174, https://doi.org/10.1021/jacs.1c12642.
- 26. S. K. Kaiser, Z. Chen, D. Faust Akl, S. Mitchell, and J. Pérez-Ramírez, "Single-Atom Catalysts Across the Periodic Table," *Chemical Reviews* 120 (2020): 11703–11809, https://doi.org/10.1021/acs.chemrev.0c00576.
- 27. Z. Chen, J. Liu, and K. P. Loh, "Engineering Single Atom Catalysts for Flow Production: From Catalyst Design to Reactor Understandings," *Accounts of Materials Research* 4 (2022): 27–41, https://doi.org/10.1021/accountsmr.2c00183.
- 28. F. G. Baddour, L. Snowden-Swan, J. D. Super, and K. M. Van Allsburg, "Estimating Precommercial Heterogeneous Catalyst Price: A Simple Step-Based Method," *Organic Process Research & Development* 22 (2018): 1599–1605, https://doi.org/10.1021/acs.oprd.8b00245.
- 29. T. J. Ross, Fuzzy Logic With Engineering Applications (John Wiley & Sons, 2005).
- 30. K. B. Cohen and L. Hunter, "Getting Started in Text Mining," *PLoS Computational Biology* 4 (2008): e20.
- 31. A. M. Aubaid and A. Mishra, "A Rule-Based Approach to Embedding Techniques for Text Document Classification," *Applied Sciences* 10 (2020): 4009.
- 32. J. Song, Z. Chen, X. Cai, et al., "Promoting Dinuclear-Type Catalysis in Cu(1)-C(3) N(4) Single-Atom Catalysts," *Advanced Materials* 34 (2022): e2204638, https://doi.org/10.1002/adma.202204638.
- 33. X. Hai, S. Xi, S. Mitchell, et al., "Scalable Two-Step Annealing Method for Preparing Ultra-High-Density Single-Atom Catalyst Libraries," *Nature Nanotechnology* 17 (2022): 174–181, https://doi.org/10.1038/s41565-021-01022-y.
- 34. L. Liu, T. Chen, and Z. Chen, "Understanding the Dynamic Aggregation in Single-Atom Catalysis," *Advanced Science* 11 (2024): e2308046, https://doi.org/10.1002/advs.202308046.
- 35. L. Laffont, M. Y. Wu, F. Chevallier, P. Poizot, M. Morcrette, and J. M. Tarascon, "High Resolution EELS of Cu–V Oxides: Application to Batteries Materials," *Micron* 37 (2006): 459–464, https://doi.org/10.1016/j.micron.2005.11.007.
- 36. T. Yang, X. Mao, Y. Zhang, et al., "Coordination Tailoring of Cu Single Sites on C_3N_4 Realizes Selective CO_2 Hydrogenation at Low Temperature," *Nature Communications* 12 (2021): 6022.
- 37. J. Song, X. Cai, Z. Chen, et al., "Expedient Alkyne Semi-Hydrogenation by Using a Bimetallic AgCu-C(3)N(4) Single Atom Catalyst," *Chemical Science* 15 (2024): 10577–10584, https://doi.org/10.1039/d4sc02469a.

- 38. W. Chen, J. Chen, K. V. Bets, et al., "Battery Metal Recycling by Flash Joule Heating," *Science Advances* 9 (2023): eadh5131, https://doi.org/10.1126/sciadv.adh5131.
- 39. A. Elshkaki, B. K. Reck, and T. E. Graedel, "Anthropogenic Nickel Supply, Demand, and Associated Energy and Water Use," *Resources, Conservation and Recycling* 125 (2017): 300–307, https://doi.org/10.1016/j.resconrec.2017.07.002.
- 40. M. Wang, A. Elgowainy, U. Lee, et al. *Summary of Expansions and Updates in GREET* (§) 2020 (Argonne National Laboratory, 2020), https://doi.org/10.2172/1671788.
- 41. X. Hai, Y. Zheng, Q. Yu, et al., "Geminal-Atom Catalysis for Cross-Coupling," *Nature* 622 (2023): 754–760, https://doi.org/10.1038/s41586-023-06529-z.
- 42. Y. Du, Y. Zhu, S. Xi, et al., "XAFCA: A New XAFS Beamline for Catalysis Research," *Journal of Synchrotron Radiation* 22 (2015): 839–843, https://doi.org/10.1107/S1600577515002854.
- 43. B. Ravel and M. Newville, "ATHENA, ARTEMIS, HEPHAESTUS: Data Analysis for X-Ray Absorption Spectroscopy Using IFEFFIT," *Journal of Synchrotron Radiation* 12 (2005): 537–541, https://doi.org/10.1107/S0909049505012719.

Supporting Information

Additional supporting information can be found online in the Supporting Information section.